Lateral pressure profiles in lipid monolayers

Baoukina, Svetlana; Marrink, Siewert J.; Tieleman, D. Peter

Published in:
Faraday Discussions

DOI:
10.1039/b905647e

Publication date:
2010

Lateral pressure profiles in lipid monolayers

Svetlana Baoukina,[a] Siewert J. Marrink[b] and D. Peter Tieleman*[a]

Received 20th March 2009, Accepted 23rd April 2009
First published as an Advance Article on the web 18th August 2009
DOI: 10.1039/b905647e

We have used molecular dynamics simulations with coarse-grained and atomistic models to study the lateral pressure profiles in lipid monolayers. We first consider simple oil/air and oil/water interfaces, and then proceed to lipid monolayers at air/water and oil/water interfaces. The results are qualitatively similar in both atomistic and coarse-grained models. The lateral pressure profile in a monolayer is characterized by a headgroup/water pressure-interfacial tension-chain pressure pattern. In contrast to lipid bilayers, the pressure decreases towards the chain free ends. An additional chain/air tension peak is present in monolayers at the air/water interface. Lateral pressure profiles are calculated for monolayers of different lipid composition under varying surface tension. Increasing the surface tension suppresses both pressure peaks and widens the interfacial tension in monolayers at the oil/water interface, and mainly suppresses the chain pressure in monolayers at the air/water interface. In monolayers in the liquid-condensed phase, the pressure peaks split due to ordering. Variation of lipid composition leads to noticeable changes in all regions of the pressure profile at a fixed surface tension.

Introduction

A typical lipid molecule consists of a polar head group and apolar long flexible hydrocarbon chains. Amphiphilic molecules self-assemble to reduce unfavorable polar–apolar contacts in a polar or apolar medium or at the interface between media of different polarity.[1] Self-assembly leads to formation of a variety of aggregates, including bilayers, monolayers, micelles, vesicles, tubes, hexagonal and cubic phases. The type of the phase formed depends on a number of factors, including the shape of the lipid molecule (*i.e.* on the effective size of the head group and chains) and the properties of the medium (polarity, geometry, *etc.*). In all phases, the headgroup/headgroup and chain/chain contacts of the neighboring lipids are separated by the hydrophobic/hydrophilic interface. Due to lipid amphiphilicity and anisotropy, the forces along the lipid molecular axis vary in nature and magnitude.[2–4] Dispersion and excluded-volume forces act between all molecular groups. Electrostatic forces originate from charges and dipoles, including hydrogen bonds and salt bridges, in the headgroups and surrounding polar solvent. In the hydrocarbon chain region, entropic interactions arise due to the restriction of accessible conformations for the lipid chains in the presence of their neighbors. The surface tension acts to shrink the hydrophobic/hydrophilic interface. This variation of interactions leads to a strongly inhomogeneous distribution of local pressures on the small length scale of the molecular size of a lipid.

[a]*Department of Biological Sciences, University of Calgary, 2500 University Dr. NW, Calgary, AB, T2N 1N4, Canada. E-mail: tieleman@ucalgary.ca*
[b]*Groningen Biomolecular Sciences and Biotechnology Institute, Zernike Institute for Advanced Materials, University of Groningen, Nijenborgh 4, 9747 AG, The Netherlands*

A lipid membrane (bilayer or monolayer) has a small thickness (~nm) relative to its lateral size (~μm) and can be thought of as a complex interface. Interfacial energy concentrated over the small thickness gives rise to local pressures of high magnitudes.[5] The local pressure distribution (from the lipid head group to the tail) along the membrane normal can be characterized by the lateral pressure profile.

The lateral pressure profile $\Pi(z)$ is defined as the difference between the lateral pressure component P_L and the normal component P_N of the pressure tensor:

$$\Pi(z) = P_L(z) - P_N \quad (1)$$

where the z-axis is directed along the membrane normal. The normal component of the pressure tensor remains constant and is equal to the pressure in the bulk; the lateral component $P_L = (P_{xx} + P_{yy})/2$ can change its amplitude and sign along z depending on the dominant interactions. Based on this definition, positive lateral pressure corresponds to repulsive interactions and negative pressure to attractive interactions. The pressure profile is a local property but is related to several macroscopic membrane properties. The sum of all interactions along the normal, or the integral of the pressure profile over the thickness, h, of the membrane, equals the surface tension with opposite sign, γ:[6]

$$\int_0^h \Pi(z)\mathrm{d}z = -\gamma \quad (2)$$

This integral is zero in a tensionless lipid bilayer in water. The first moment of the pressure profile (in a flat membrane) gives the product of the membrane bending modulus, k_b, and spontaneous curvature, c_0: $\int_0^h \Pi(z)z\mathrm{d}z = k_b c_0$, and the second moment of the pressure profile equals the saddle-splay modulus: $\int_0^h \Pi(z)z^2\mathrm{d}z = k_G$.[7] While the lateral pressure profile is difficult to assess experimentally (due to the strong variation of local pressure on a very small length scale), these macroscopic properties are measurable quantities.

Lateral pressure profiles in lipid bilayers are of specific interest because they can influence the function of proteins in cell membranes.[8] If the protein activity involves non-uniform changes in its cross-sectional area, then variations in the bilayer lateral pressure profile can shift the protein conformational equilibrium.[9] Perturbations of bilayer lateral pressure induced by small amphiphilic solutes have been proposed as a mechanism of general anesthesia.[10–12] Lateral pressure profiles in lipid bilayers have been extensively studied using theoretical and computational approaches.[7,13–25] Theoretical models are usually based on a mean-field approximation and focus on descriptions of the hydrocarbon chain conformations in a lattice or continuum representation. The head groups are not treated explicitly; their contribution enters as a function of the lipid surface density (or area per lipid). Hydrophobic/hydrophilic interactions are localized at the interface by setting an effective interfacial tension. These models allow calculation of the lateral pressure profile in the hydrocarbon chain region for pure or multi-component bilayers.

While theoretical models can take into account such properties as the magnitude of interfacial tension, head group repulsion, and length and unsaturation of the hydrocarbon chains, they still lack molecular details. Computer simulations can provide an atomic level of detail and explicitly include all intermolecular interactions. Molecular dynamics (MD) simulations have been used to investigate lateral pressure profiles in lipid bilayers of varying composition, containing sterols,[26]

alcohols,[27,28] and poly-unsaturated hydrocarbon chains.[29] In a recent study,[30] a 3D pressure profile was calculated and a position dependent pressure distribution across the interface was obtained in bilayers with coexisting gel and liquid-crystalline phases, at finite curvature, and with embedded proteins.

In this work, we use MD simulations to study lateral pressure profiles in lipid monolayers. A lipid monolayer is not a mere half of a bilayer: it is formed in anisotropic conditions at a polar/apolar interface, and its properties vary with the surface density, which regulates the total surface tension at the interface. Previous simulation studies investigated monolayers of various surfactants.[31–44] However, the lateral pressure distribution across the monolayer at the interface, to our knowledge, was not calculated before. Here we focus on characterizing the lateral pressure profiles in lipid monolayers at the air/water and oil/water interfaces. To obtain more insight into the nature of pressure distributions at these complex interfaces, we first consider simple oil/air and oil/water interfaces. We then investigate lipid monolayers of different composition under varying surface tension. We compare the pressure profiles for an atomistic model and a coarse-grained model (CG). While the nature and relative contribution of interaction types in the two models differ, in particular in the headgroup/water region, both models yield qualitatively similar results. In comparison to lipid bilayers, in monolayers an additional tension peak appears at the chain/air interface. Upon transformation from the liquid-expanded to the liquid-condensed phase, this tension is compensated by positive pressure due to an increased chain density, and the profile is characterized by multiple peaks originating from ordering. Variation of the surface tension induces pressure re-distribution in monolayers at both air/water and oil/water interfaces. Spontaneous curvature of the constituting lipids affects all regions of the pressure profile at a fixed surface tension.

Methods

Simulation details

We simulated 'pure' oil/air and oil/water interfaces, as well as lipid monolayers at these air/water and oil/water interfaces. For comparison with previous work, we also simulated lipid bilayers in water. Simulations were performed with the GROMACS (version 3.3.3) software package[45] using atomistic and coarse-grained (CG) models. All systems were simulated at 310 K (except for a bilayer in the CG model at 270 K to obtain the gel phase) and coupled to a Berendsen heat bath.[46] In the CG model, the coupling constant was 1.0 ps; each monolayer, water (with ions) and oil were included in separate temperature coupling groups. In the atomistic model, the coupling constant was 0.1 ps; molecules of each type from each monolayer were coupled to a separate group. The Berendsen algorithm was used for pressure coupling with a time constant of 4.0 ps in the CG model and 1.0 ps in the atomistic model using the coupling schemes as indicated below. To test the effect of the weak coupling algorithm on the calculated lateral pressure profiles, we also performed simulations with the Nose–Hoover thermostat[47,48] and Parrinello–Rahman barostat,[49] which did not lead to any noticeable changes in the results. This is to be expected as we only use average properties, not the fluctuations in temperature or pressure. The simulations were 1 μs long for the CG model (actual simulation time) and 200 ns long for the atomistic model. The initial 20 ns of each atomistic run were used for equilibration.

Simple interfaces

For simulations of the oil/air and oil/water interfaces, the system setup consisted of an oil slab in vacuum, and water and oil slabs, respectively. Hexadecane molecules were used as oil. To simulate the ordered oil/air interface, position restraints were applied to the first particle in each oil chain; the box lateral size was chosen to approximate the density of the disordered oil. No pressure coupling was used for the oil slab in vacuum. The oil/water interface was coupled to the normal pressure

of 1 bar; the box size in lateral direction (parallel to the slabs) was kept constant. The systems included 144 oil molecules, 688 water particles in the CG model and 3255 water molecules in the atomistic model.

Monolayers

The system setup consisted of a water slab in vacuum or oil with two symmetric monolayers at the two polar/apolar interfaces. Surface tensions in the range 0–40 mN/m were applied using the surface-tension coupling scheme. Compressibility in the normal direction was set to zero in the case of the air/water interface; normal pressure was set to 1 bar in the case of the oil/water interface. The following lipid compositions were simulated in the CG model: pure dipalmitoyl-phosphatidylcholine (DPPC), pure diarachidonoyl-phosphatidylcholine (DAPC), a mixture of DPPC and the lyso-lipid palmitoyl-phosphatidylcholine (PPC) in a 1 : 1 ratio, and a mixture of DPPC and palmitoyloleoyl-phosphatidylglycerol (POPG) in a 3 : 1 ratio. In the atomistic model we simulated pure DPPC monolayers. Each monolayer consisted of 36 lipids in all small systems and of 4096 lipids in larger systems in the CG model. Small systems included between 800 and 1220 water particles (depending on the lipid mixture) in the CG model, and 3000 water molecules in the atomistic model. The large system included 150 289 water particles. Na^+ ions were added to compensate for the negative charge of POPG lipids. The system with DPPC monolayers at the oil/water interface in the CG model contained 288 oil molecules.

Bilayers

DPPC bilayers in water were simulated at 310 K and 270 K in the CG model. The system contained 72 lipids and 800 water particles. A semi-isotropic pressure coupling scheme was used with normal and lateral pressures of 1 bar.

Coarse-grained (CG) force field

We used the MARTINI coarse-grained force field for lipids.[50,51] In this model, the molecules are represented by grouping four heavy atoms (two to three in the case of ring structures) into a particle. All considered lipids are standard components of this force field, except for POPG for which the glycerol group in the headgroup was represented by a polar particle (P4). To model less hydrophobic oil, the particles in hexadecane (C1) were substituted by less apolar ones (C5). For non-bonded interactions, the standard cutoffs for the CG force field were used: the Lennard–Jones interactions were shifted to zero between 0.9 and 1.2 nm, the Coulomb potential was shifted to zero between 0 and 1.2 nm. The relative dielectric constant was 15, which is the default for this force-field.[50] A time step of 20 fs was used; the neighbor list was updated every 10 steps.

Atomistic force field

For the DPPC lipids, bonded and non-bonded parameters of lipid tails are adopted from the Berger model[52] with charges from Chiu.[53] Bonded parameters are based on the GROMOS force field;[54] non-bonded parameters are based on the OPLS united atom force field.[55] The headgroup charges were reduced to reproduce the LC phase in monolayers at a surface tension of 0 mN/m. Hexadecane was simulated using Berger parameters. Water was simulated using the SPC model[56] and flexible SPC model where specified. Bonds were constrained with the LINCS algorithm[57] for lipids and the SETTLE algorithm[58] for water. For Lennard–Jones interactions, a cut-off of 1 nm was used. For electrostatic interactions, a cut-off of 1.4 nm was combined with the reaction field method for long-range electrostatics with a dielectric constant of 54, the dielectric constant of SPC water. A time step of 2 fs was used, the neighbor list was updated every 10 steps.

Calculation of the lateral pressure profile

The calculation of lateral pressure was carried out using a procedure analogous to ref. 19. For a system of point-like particles interacting through pair-wise forces the macroscopic pressure tensor is given by:

$$\mathbf{P} = \frac{1}{V}\Big(\sum_i m_i \mathbf{v}_i \otimes \mathbf{v}_i - \sum_{i<j} \mathbf{F}_{ij} \otimes \mathbf{r}_{ij}\Big) \tag{3}$$

where m, $\mathbf{v}$, $\mathbf{r}$ and $\mathbf{F}$ are masses, velocities, distances and forces between the particles, respectively. The first term represents the kinetic contribution and the second term is the configurational contribution from the interactions in the volume V. On the scale of molecular interactions, the configurational contribution to the local pressure is defined through the (arbitrary) contour C_{ij} connecting two particles:[59]

$$\boldsymbol{\sigma}(\mathrm{r}) = -\frac{1}{2}\sum_{i<j} \mathbf{F}_{ij} \int_{C_{ij}} \delta(\mathbf{r}' - \mathbf{I})\mathrm{ds} \tag{4}$$

We use the Irving–Kirkwood contour, which connects the pair of interacting particles *via* a straight line. The simulation box is divided into slices of 0.1 nm thickness perpendicular to the z-axis, and the configurational stress tensor is found as a function of z:

$$\boldsymbol{\sigma}(z) = \frac{1}{\Delta \mathrm{V}}\sum_{i<j} \mathbf{F}_{ij} \otimes \mathbf{r}_{ij} \mathrm{f}\big(z, z_i, z_j\big) \tag{5}$$

where $\mathrm{f}(z,z_i,z_j)$ is the weighting function depending on the position of the particles with respect to the given slice and ΔV is the volume of the slice.

To calculate the pressure profiles we performed reruns of the trajectories with a modified version of GROMACS which calculates the local pressure tensor in the form of eqn (5). For each slice the pressure tensor was evaluated every 20 ps. The SHAKE algorithm[60] was used for reruns, as LINCS does not directly yield pair-wise forces.[19]

Results

Simple interfaces

To obtain more insight into the nature of the lateral pressure profile in a complex monolayer-covered polar/apolar interface, we first calculated the distribution of lateral pressure for simple interfaces. To this end, we simulated oil/water and oil/air interfaces, the latter for both disordered and ordered hexadecane chains. The lateral pressure profile for a disordered oil/air interface in the CG and atomistic models is shown in Fig. 1a. Negative pressure originates from a positive surface tension (eqn (2)), penalizing exposure of hydrocarbon chains to air. Note that the surface tension of the chain/air interface in the atomistic model (~12 mN/m) is smaller than that in the CG model (~24 mN/m). The lateral pressure distribution for the oil/water interface in the CG and atomistic models is shown in Fig. 1b. Interestingly, the profile is characterized by two negative peaks in the case of the CG model. This is because in this model the surface tension at the oil/water interface (~42 mN/m) is larger than both the surface tension of the oil/air interface and of the air/water interface (~32 mN/m). The first two tensions reproduce well the experimental data; the surface tension at the air/water interface in the CG model is lower than in the atomistic model (~53 mN/m) and than the experimental value (~70 mN/m at 310 K). The least favorable oil/water interface in the CG model thus splits into two with lower tensions. This effect can be removed by substituting the

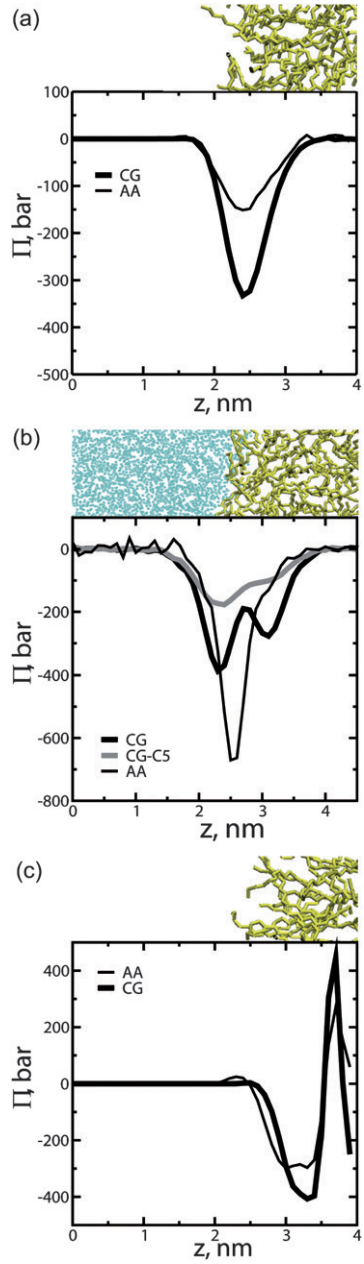

Fig. 1 Lateral pressure profile for simple interfaces in the coarse-grained (CG) and atomistic (AA) models: (a) oil/air, (b) oil/water, (c) ordered oil/water. Oil chains are shown as sticks, water particles as spheres.

oil particles by less hydrophobic ones (see Methods) which lowers the oil/water surface tension (to ~21 mN/m). For the ordered oil/air interface (see Methods), the pressure profile has an additional positive peak originating from an increased density of the hexadecane segments in the imposed orientation normal to the interface, see Fig. 1c.

Monolayer at oil/water interface

The lateral pressure profile for a DPPC monolayer at the oil/water interface (CG model) is shown in Fig. 2. The pressure distribution in the head group region and at the hydrophobic/hydrophilic interface is similar to that of a (DPPC) bilayer. The minimum of negative pressure of the hydrophobic/hydrophilic interface falls into the region where the chain and water density distribution overlap, corresponding to the glycerol/ester region. In the hydrocarbon chain region, in contrast to bilayers, the pressure decreases towards the chain ends. One can distinguish two factors determining the pressure distribution in the chain region: entropic repulsion due to restriction of conformational freedom of the chains, and deviation of chain density from that in the bulk. Entropic repulsion of the flexible chains oriented along the molecular axis increases towards the free ends due to the disorder gradient.[61] In bilayers, this entropic contribution usually dominates as the density of the oriented chains remains high. In the limit of vanishing chain bending stiffness (with no bond angle potentials in the CG model) the chains would lose their preferred orientation, and the pressure in the bilayer center would decrease (results not shown). The requirement of constant density of chain segments in mean-field theoretical models also effectively disorders the chains and leads to a reduction of lateral pressure in the bilayer center. In monolayers, the density of oriented chains decreases noticeably towards the ends. Disordered oil from the bulk partially penetrates the ordered chain region (Fig. 2), and the pressure gradually assumes its bulk value.

Monolayer at air/water interface

The lateral pressure distribution for a DPPC monolayer at the air/water interface is shown in Fig. 3. In contrast to a monolayer at an oil/water interface, the pressure at

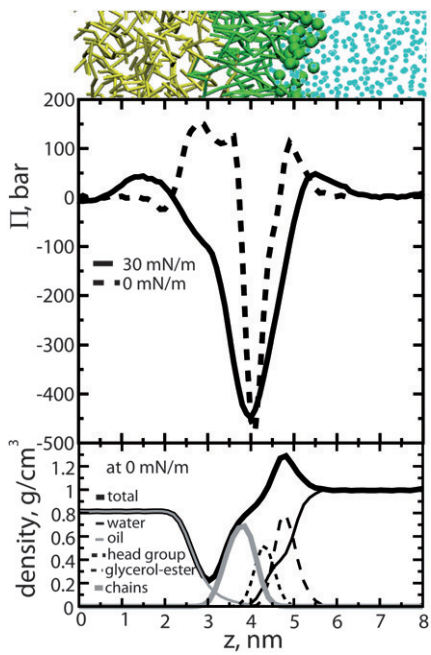

Fig. 2 Distribution of lateral pressure and density for a DPPC monolayer at the oil/water interface in the coarse-grained model. Lateral pressure profiles are shown at surface tensions of 0 and 30 mN/m, the partial density only at 0 mN/m. Lipids are shown as sticks, the head-group particles are marked as spheres, oil and water as in Fig. 1.

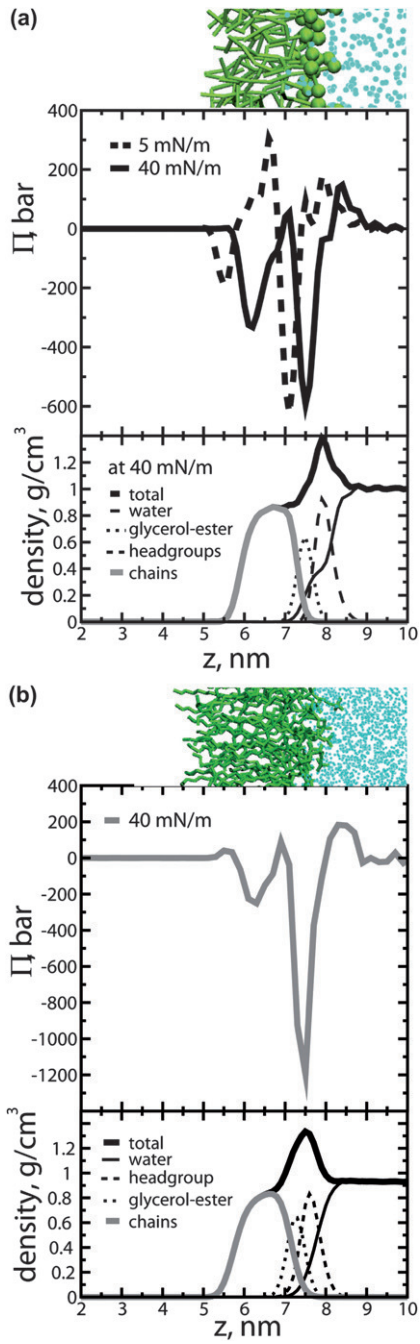

Fig. 3 Distribution of lateral pressure and density for a DPPC monolayer in the LE phase at the air/water interface in the coarse-grained (a) and atomistic (b) models. Lipids are shown as sticks (with the headgroup particles marked as spheres in the coarse-grained model), spheres represent each water atom in the atomistic model and four water molecules in the coarse-grained model.

the chain ends becomes negative. The surface tension at the chain/air interface and a decrease of total density towards the chain ends suppress entropic repulsion. The profiles in the atomistic and CG models are qualitatively similar. Headgroup/solvent interactions are repulsive in total, due to an increased density of the perturbed water in the CG model (Lennard–Jones water/headgroup interactions are stronger than water/water interactions) and ordering of water dipoles in the atomistic model. Headgroup/headgroup interactions are overall attractive in the atomistic model due to partial screening of headgroup dipoles and hydrogen bonding. In the CG model, repulsive interactions between headgroup charges are (partially) compensated by attractive Lennard–Jones interactions with waters solvating the headgroups. As a result of the differences in electrostatic interactions and water representations, the CG and atomistic profiles differ quantitatively in the headgroup/perturbed water and interfacial regions.

Surface tension

A change in surface tension, which changes the monolayer surface density from expanded to compressed, has strong effects on the monolayer pressure profile, both at the oil/water and at the air/water interface. For the monolayer at the oil/water interface (Fig. 2), an increase in surface tension (or decrease in surface density) reduces the magnitude of the pressure in the head group and chain regions. At the same time, the pressure peak corresponding to the hydrophobic/hydrophilic interface significantly widens. Upon increasing the surface tension, the system thus transforms into a single oil/water interface. For the monolayer at the air/water interface (Fig. 3a), a larger surface tension suppresses the pressure in the chain region and between the headgroups, while the pressure peaks at the headgroup/solvent and interfacial regions do not change noticeably. In bilayers, increasing the area per lipid was found to lower the pressure in the chain region and increase interfacial tension.[21] Increasing the bulk pressure, on the other hand, suppressed the pressure magnitudes in all regions in a non-uniform manner.[27] Correspondence of the lateral pressure shifts in bilayers and monolayers likely also depends on the degree of membrane stretching/compression. Besides the above mentioned changes, variation of surface tension and density can induce phase transitions in monolayers.

Phase behavior

We simulated the transition from the liquid-expanded (LE) to the liquid-condensed (LC) phase for the DPPC monolayer at the air/water interface by reducing the surface tension to 0 mN/m. The pressure profile of the LC monolayer (Fig. 4) is characterized by multiple peaks, analogous to a bilayer in the gel phase.[30] In contrast to the LE phase, the pressure at the chain/air interface is positive as a result of the higher chain density. The negative pressure peak from chain ends is shifted towards the mid-chain region. A change in sign of the lateral pressure in the chain region is also similar to a liquid-ordered bilayer with high cholesterol concentration.[30,62] Ordering of the headgroups and adjacent water in the CG model increases oscillations in the density (see Fig. 4a). In the atomistic model (Fig. 4b), the total density of the perturbed water layer does not change noticeably. The headgroup dipoles increase the ordering of the adjacent water dipoles (results not shown), which appears to lead to stronger repulsion in the perturbed water layer. Due to the higher monolayer surface density, solvation of headgroups by water is lower in the LC phase compared to the LE phase. This decreases the electrostatic screening in the atomistic model and attractive headgroup/water interactions in the CG model. This in turn increases the contribution of repulsive electrostatic interactions between the headgroups, which leads to an additional pressure peak in the CG model and a smaller tension in the atomistic model. Combining the CG and atomistic results,

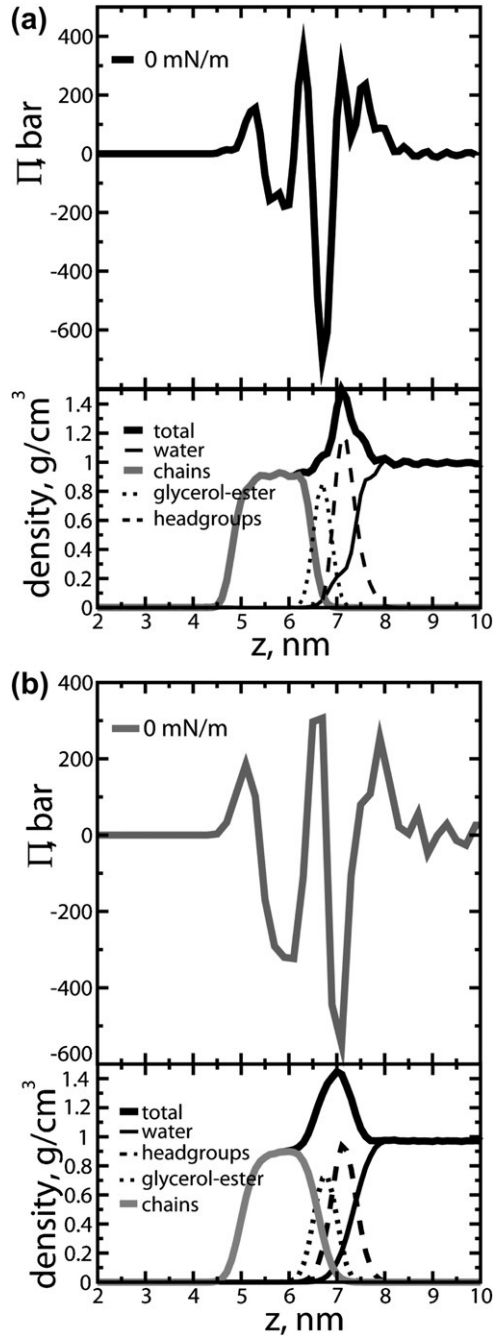

Fig. 4 Distribution of lateral pressure and density for a DPPC monolayer in the LC phase at the air/water interface in the coarse-grained (a) and atomistic (b) models.

the monolayer pressure profile in the LC phase is distinct from that in the LE phase by splitting of the peaks due to ordering and increased density, and repulsive pressure at the chain/air interface.

System size

To test the effect of system size on the calculated pressure distribution in monolayers, we simulated larger systems. This effect can be best demonstrated on a system forming the LE phase (with low bending rigidity) at low surface tension, with the ability to sustain near-zero tension, undergoing strong thermal undulations. As an example of a system with such properties in the CG model, we considered the mixture of DPPC and palmitoyloleoyl-phosphatidylglycerol (POPG) in a 3 : 1 ratio. A comparison between the lateral pressure distribution in a small (36 lipids) and large (4096 lipids) monolayer is shown in Fig. 5. High pressure peaks resolved in the small system are averaged out in the large system due to out-of-plane fluctuations of the monolayer. This favors the use of smaller over larger systems for the calculation of the pressure profiles, if the correct properties in the former can be reproduced (*e.g.* for the laterally homogenous membranes).

Lipid spontaneous curvature

To investigate the influence of spontaneous curvature on the monolayer pressure profile, we simulated cone and inverted-cone shaped lipids, the mixture of DPPC and single chain palmitoyl phosphatidylcholine (PPC) lipids in a 1 : 1 ratio and polyunsaturated diarachidonoyl phosphatidylcholine (DAPC) lipid (in the CG model), respectively. The pressure distributions at a surface tension of 20 mN/m are shown in Fig. 6. The pressure profile in the DPPC : PPC 1 : 1 mixture has smaller peaks in the interfacial and chain regions, as compared to pure DPPC monolayer. The magnitude of the head group peak, however, did not increase, likely due to lower compressibility of the head groups than the chains. In the DAPC monolayer, the pressure becomes dominant in the chain region. Simultaneously, the hydrophobic/hydrophilic interfacial peak decreases noticeably due to the presence of the less hydrophobic unsaturated chain segments. Polyunsaturation of one of the two hydrocarbon chains in (atomistic) bilayers was found to increase the magnitude of the interfacial tension, and to suppress the entropic pressure in the bilayer center.[29] Changes in lipid composition can be expected to have different effects on the lateral pressure distribution in bilayers and monolayers, because of the monolayer asymmetric environment and varying surface density or surface tension. For a monolayer at a fixed surface tension, changes in the lipid hydrocarbon chains which affect the effective size of the chains *versus* the headgroups can introduce noticeable shifts (~100 bar) in all regions of

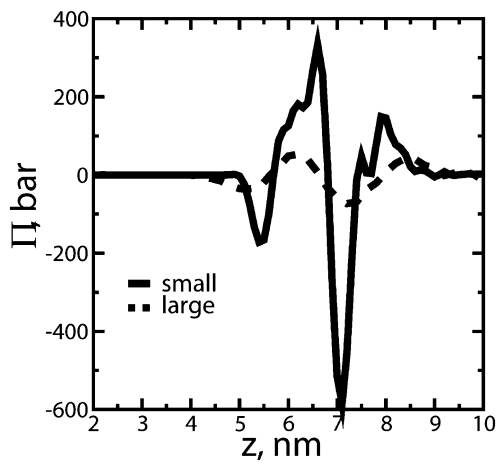

Fig. 5 Lateral pressure profile for a small (36 lipids) and large (4096 lipids) monolayer of DPPC and POPG at the air water interface in a 3 : 1 ratio at a surface tension of 0 mN/m.

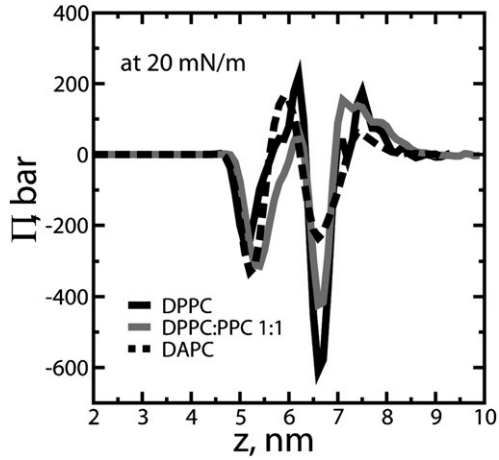

Fig. 6 Lateral pressure profile for DPPC, DPPC : PPC in a 1 : 1 ratio and DAPC monolayers at the air/water interface at a surface tension of 20 mN/m.

the pressure profile. We also calculated the first moment of the pressure profile for these systems at a surface tension of 20 mN/m. As the reference position, we chose the minimum of the tension peak of the hydrophobic/hydrophilic interface. While this choice is arbitrary, it seems logical for assessing relative contributions of the chains and headgroups. The calculated values are 200, 200 and 370 bar·nm^2, for the DPPC, DAPC, and DPPC : PPC mixtures, respectively. Using an estimate of the monolayer bending modulus as $k_b \sim k_A \cdot d^2$, allows characterizing qualitatively the monolayer spontaneous curvature from the fist moment of the pressure profile (see Introduction). Here d is the length of the hydrocarbon chains, and the k_A is the monolayer area compression modulus found from the slope of the monolayer tension-area isotherm in simulations using the formula: $k_A = A_m \partial \gamma_m / \partial A_m$, and A_m is the monolayer area. These estimates give bending moduli of 6, 2 and 5 $\times 10^{-19} J$ and spontaneous curvatures of 0.03, 0.1 and 0.07 nm^{-1}, for the DPPC, DAPC, and DPPC : PPC mixtures, respectively. The monolayer spontaneous curvature clearly depends on the choice of the reference plane and the surface density. Spontaneous curvatures of bilayer leaflets with respect to the bilayer center (in the same CG model) were found[50] to have negative values of comparable magnitudes. Here, all values are positive, even for the DAPC monolayer, which intuitively might be expected to have a negative spontaneous curvature because of the large volume of the unsaturated chains. On the other hand, a positive curvature may be explained by the tendency of polyunsaturated chains to back fold towards the interface observed in liposomes.[63] It is interesting to note that subtracting the chain/air interfacial peak (as obtained for simple chain/air interface) from the monolayer pressure profile results in a negative spontaneous curvature for DPPC and DAPC monolayers (results not shown).

Discussion

We calculated the lateral pressure profiles in a number of interfacial systems, including lipid monolayers, using both CG and atomistic simulations. Previous simulations have extensively studied the pressure profiles in lipid bilayers.

Similar to that of a lipid bilayer, the monolayer pressure profile is characterized by the headgroup/water pressure- interfacial tension–hydrocarbon chain pressure pattern. In contrast to the symmetric conditions of a bilayer, this positive-negative-positive pressure distribution in monolayers is required to balance the bending moments ($\sim \Pi \cdot z$) at the asymmetric interface.

Unlike in lipid bilayers, the pressure decreases towards chain ends in monolayers at the oil/water interface, and an additional chain/air tension peak appears in monolayers at the air/water interface. As with other monolayer properties, the pressure profile in the monolayer depends on the surface density, which determines the total surface tension at the interface. For a monolayer at the oil/water interface, reduction of the surface density widens the interfacial tension region, and suppresses both pressure peaks. For a monolayer at the air/water interface, reduction of the surface density mainly suppresses the chain pressure. A transition from the LE to the LC phase, which can be induced by lowering the total surface tension (or temperature), is characterized by splitting of the pressure peaks in the ordered monolayer.

The shape of the pressure profile can be understood by considering the nature of interactions between different molecular groups. In an earlier simulation study of atomistic bilayers by Lindahl and Edholm,[19] the pressure profile was decomposed into interactions of different origins (including Lennard–Jones, electrostatic, bonded and 1–4 interactions), between headgroups, chains and water, separating entropic and enthalpic contributions. The profile was shown to represent a sum of an order of magnitude larger terms of opposing sign. These terms depend on the simulation force field/details, and their balance is required for the equilibrium structure. Mismatch of these interactions in the simulation setup can lead to a system with incorrect properties (*e.g.* a bilayer with underestimated area per lipid) or to non-lamellar phases. If a monolayer/bilayer with correct properties and phase behavior can be formed, the distribution of lateral pressure is expected to be almost independent of the details, as the self-assembled soft matter is governed by entropic interactions, which are mainly determined by molecular size and shape.

In the atomistic and CG models used in this study, several interactions are different. In comparison to the atomistic model, the CG model does not include explicitly the chain dihedral potentials, carbonyl dipoles, water dipoles, hydrogen bonds, *etc.* The calculated pressure profiles in monolayers in these two models are qualitatively similar, because the CG model appears to capture an essential fraction of the lipid/solvent properties. In the hydrophobic part, the dominating contribution to the profile is the conformational entropy of the chains, which increases towards free ends. This would not be the case for a simpler model with short (*e.g.* two-bead) chain(s) or with zero chain bending stiffness, see the results of Venturoli and Smit[16]). In the headgroups, the treatment of electrostatics in atomistic models may result in overall attractive or repulsive interactions, depending on the distribution of partial charges and the treatment of electrostatic interactions in the simulation, compare previous results.[19,21,26,27] In the absence of charges, the pressure distribution in the headgroup and perturbed water regions would be determined only by the Lennard-Jones/conservative force parameters. Overall, the model parameters can modulate the magnitude and sign of selected pressure regions to an extent comparable to variations in lipid composition. Including more interaction levels, for example, polarizability, can further refine the pressure distribution.

Limitations

We investigated a number of technical limitations of the pressure profile calculations. It is important to keep in mind that a certain range of conditions (*e.g.* surface tensions) applied to systems of small size ($\sim$5nm) can correspond to an unphysical state. For example, phase separation cannot be studied and collapse surface tension cannot be assessed using small monolayers. For the long-range electrostatic interactions with the PME scheme, the local pressure integration algorithm with the Irving–Kirkwood contour requires approximations with a cut-off scheme.[64] For this reason we used the RF scheme in all atomistic simulations with long-range electrostatics (see Methods). Another source of errors is the constraint force calculation procedure in the trajectory post-analysis.[19,65] As a test for the validity of the calculated profiles, the integral of the pressure profile is required to converge to the total surface tension

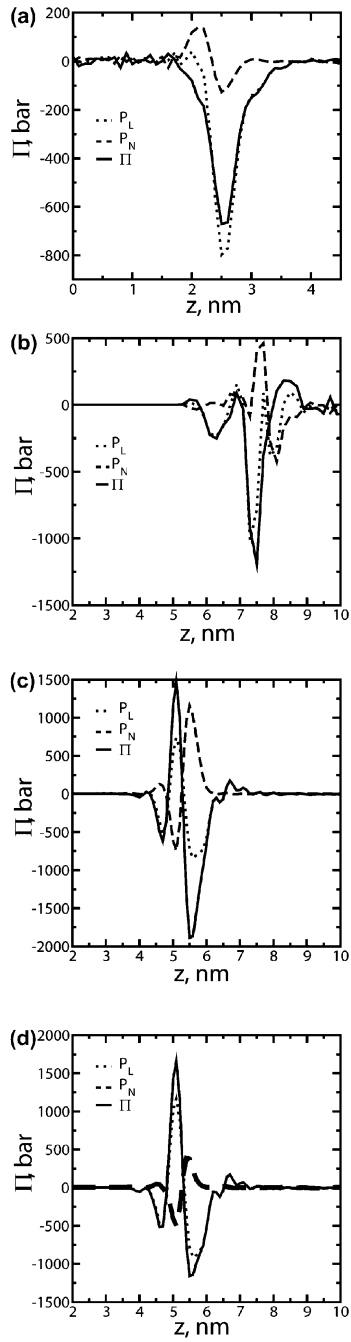

Fig. 7 Distribution of the normal (P_N) and lateral (P_L) pressures and the lateral pressure profile (Π) for (a) the atomistic oil/water interface; (b) an atomistic DPPC monolayer at the air/water interface at a surface tension of 40 mN/m; (c) a coarse-grained monolayer of DPPC : POPG : cholesterol in a 4 : 1 : 4 ratio at a surface tension of 40 mN/m; (d) system as in (c) with constraints in the cholesterol bonds substituted by a harmonic bond potential.

at the interface (with opposite sign, see eqn (2)), and the normal pressure is required to remain constant to satisfy the mechanical equilibrium condition. The normal pressure across the interface deviated from the bulk value in a number of calculated profiles. This was the case for all simulations with constraints for molecular bonds, if orientational ordering of molecular groups with respect to the interface normal was present. The normal pressure across the atomistic oil/water interface (Fig. 7a) is constant at the (disordered) hexadecane boundary but fluctuates at the water boundary as the water dipoles are ordered due to the hydrophobic effect. Using harmonic potential for the bonds in the water model (see Methods) restored the normal pressure to the bulk value.

Deviations of the normal pressure from the bulk are even stronger when a lipid monolayer is present at the interface (Fig. 7b), where molecular segments have a preferred orientation with respect to the monolayer normal. The same effect is observed in the CG monolayer with a high concentration of cholesterol (DPPC : POPG : cholesterol in ratio 4 : 1 : 4), in which several bonds are modeled with constraints, see Fig. 7c. Substituting constraints by the harmonic bonds noticeably reduced the normal pressure (Fig. 7d), but did not provide the bulk value, possibly because of distortions of the cholesterol ring structure. At the same time, the integral of the pressure profile did not converge to the total surface tension in most cases. While in the atomistic systems this could be attributed to the large fluctuations in pressure due to insufficient sampling, this clearly should not be the case in the CG systems. In all systems with non-constant normal pressure across the interface, the contribution of normal pressure is comparable in magnitude to the lateral pressure, and affects significantly the lateral pressure distribution. Due to these factors, the results presented in this work rely mainly on the CG model without constraints.

Implications

In conclusion, we outline the potential significance of the lateral pressure profile in lipid monolayers covering oil/water or air/water interfaces. In such complex interfaces, the "surface of tension" can be determined from the first moment of the pressure profile:[7]

$$\int_0^h \Pi(z)(z - z_0)\mathrm{d}z = 0 \tag{6}$$

Here the integral is proportional to the total bending moment across the interface, and the reference coordinate z_0 is chosen such that the integral becomes zero. We hypothesize that the location of this surface of tension z_0 is related to the stability of the monolayer at a given surface tension, and will pursue a verification of this hypothesis in a further study.

Acknowledgements

SB is supported by postdoctoral fellowships from the Alberta Heritage Foundation for Medical Research (AHFMR) and the Canadian Institutes for Health Research (CIHR). DPT is an AHFMR Senior Scholar and CIHR New Investigator. This work was supported by the Natural Sciences and Engineering Research Council (Canada).

References

1 C. Tanford, *The hydrophobic effect*, Wiley, New York, 1980.
2 J. N. Israelachvili, *Intermolecular and Surface Forces*, Academic Press, London, 1985.
3 D. Marsh, *Biochim. Biophys. Acta*, 1996, **1286**, 183–223.

4 A. Ben-Shaul, Elsevier, Amsterdam, 1995.
5 G. L. Gaines, *Insoluble Monolayers at Liquid-Gas Interfaces*, Wiley (Interscience), New York, 1966.
6 J. S. Rowlinson and B. Widom, *Molecular Theory of Capillarity*, Clarendon, Oxford, 1982.
7 I. Szleifer, D. Kramer, A. Benshaul, W. M. Gelbart and S. A. Safran, *J. Chem. Phys.*, 1990, **92**, 6800–6817.
8 B. de Kruijff, *Nature*, 1997, **386**, 129–130.
9 R. S. Cantor, *J. Phys. Chem. B*, 1997, **101**, 1723–1725.
10 R. S. Cantor, *Biophys. J.*, 1997, **72**, A43.
11 S. M. Gruner and E. Shyamsunder, *Mol. Cell. Mech. Alcohol Anesth.*, 1991, **625**, 685–697.
12 J. M. Seddon and R. H. Templer, Elsevier, Amsterdam, 1995.
13 R. Goetz and R. Lipowsky, *J. Chem. Phys.*, 1998, **108**, 7397–7409.
14 T. X. Xiang and B. D. Anderson, *Biophys. J.*, 1994, **66**, 561–572.
15 D. Harries and A. BenShaul, *J. Chem. Phys.*, 1997, **106**, 1609–1619.
16 M. Venturoli and B. Smit, *PhysChemComm*, 1999, **2**, 45–49.
17 R. S. Cantor, *Toxicol. Lett.*, 1998, **101**, 451–458.
18 R. S. Cantor, *Biophys. J.*, 1999, **76**, 2625–2639.
19 E. Lindahl and O. Edholm, *J. Chem. Phys.*, 2000, **113**, 3882–3893.
20 J. C. Shillcock and R. Lipowsky, *J. Chem. Phys.*, 2002, **117**, 5048–5061.
21 J. Gullingsrud and K. Schulten, *Biophys. J.*, 2004, **86**, 3496–3509.
22 S. I. Mukhin and S. Baoukina, *Phys. Rev. E: Stat., Nonlinear, Soft Matter Phys.*, 2005, **71**.
23 M. Patra, *Eur. Biophys. J. Biophys. Lett.*, 2005, **35**, 79–88.
24 M. Carrillo-Tripp and S. E. Feller, *Biochemistry*, 2005, **44**, 10164–10169.
25 A. L. Frischknecht and L. J. D. Frink, *Biophys. J.*, 2006, **91**, 4081–4090.
26 O. H. S. Ollila, T. Rog, M. Karttunen and I. Vattulainen, *J. Struct. Biol.*, 2007, **159**, 311–323.
27 B. Griepernau and R. A. Bockmann, *Biophys. J.*, 2008, **95**, 5766–5778.
28 E. Terama, O. H. S. Ollila, E. Salonen, A. C. Rowat, C. Trandum, P. Westh, M. Patra, M. Karttunen and I. Vattulainen, *J. Phys. Chem. B*, 2008, **112**, 4131–4139.
29 S. Ollila, M. T. Hyvonen and I. Vattulainen, *J. Phys. Chem. B*, 2007, **111**, 3139–3150.
30 O. H. S. Ollila, H. J. Risselada, E. Lindahl, I. M. Vattulainen and S.J., *Phys. Rev. Lett.*, 2009, in press.
31 P. Ahlstrom and H. J. C. Berendsen, *J. Phys. Chem.*, 1993, **97**, 13691–13702.
32 Y. N. Kaznessis, S. T. Kim and R. G. Larson, *Biophys. J.*, 2002, **82**, 1731–1742.
33 V. Knecht, M. Muller, M. Bonn, S. J. Marrink and A. E. Mark, *J. Chem. Phys.*, 2005, **122**, 024704.
34 S. O. Nielsen, C. F. Lopez, P. B. Moore, J. C. Shelley and M. L. Klein, *J. Phys. Chem. B*, 2003, **107**, 13911–13917.
35 H. Dominguez, A. M. Smondyrev and M. L. Berkowitz, *J. Phys. Chem. B*, 1999, **103**, 9582–9588.
36 J. I. Siepmann, S. Karaborni and M. L. Klein, *J. Phys. Chem.*, 1994, **98**, 6675–6678.
37 S. Baoukina, L. Monticelli, S. J. Marrink and D. P. Tieleman, *Langmuir*, 2007, **23**, 12617–12623.
38 S. L. Duncan and R. G. Larson, *Biophys. J.*, 2008.
39 C. F. Lopez, S. O. Nielsen, P. B. Moore, J. C. Shelley and M. L. Klein, *J. Phys.: Condens. Matter*, 2002, **14**, 9431–9444.
40 D. Rose, J. Rendell, D. Lee, K. Nag and V. Booth, *Biophys. Chem.*, 2008, **138**, 67–77.
41 A. Gupta, A. Chauhan and D. I. Kopelevichc, *J. Chem. Phys.*, 2008, 128.
42 S. Baoukina, L. Monticelli, M. Amrein and D. P. Tieleman, *Biophys. J.*, 2007, **93**, 3775–3782.
43 S. Baoukina, L. Monticelli, H. J. Risselada, S. J. Marrink and D. P. Tieleman, *Proc. Natl. Acad. Sci. U. S. A.*, 2008, **105**, 10803–10808.
44 C. Laing, S. Baoukina and D. P. Tieleman, *Phys. Chem. Chem. Phys.*, 2009, **11**, 1916–1922.
45 E. Lindahl, B. Hess and D. van der Spoel, *J. Mol. Model.*, 2001, **7**, 306–317.
46 H. J. C. Berendsen, J. P. M. Postma, W. F. van Gunsteren, A. DiNola and J. R. Haak, *J. Chem. Phys.*, 1984, **81**, 3684–3690.
47 W. G. Hoover, *Phys. Rev. A*, 1985, **31**, 1695–1697.
48 S. Nose, *Mol. Phys.*, 1984, **52**, 255–268.
49 M. Parrinello and A. Rahman, *J. Appl. Phys.*, 1981, **52**, 7182–7190.
50 S. J. Marrink, H. J. Risselada, S. Yefimov, D. P. Tieleman and A. H. Vries, *J. Phys. Chem. B*, 2007, **111**, 7812–7824.
51 L. Monticelli, S. K. Kandasamy, X. Periole, R. G. Larson, D. P. Tieleman and S. J. Marrink, *J. Chem. Theory Comput.*, 2008, **4**, 819–834.
52 O. Berger, O. Edholm and F. Jahnig, *Biophys. J.*, 1997, **72**, 2002–2013.

53 S. W. Chiu, M. Clark, V. Balaji, S. Subramaniam, H. L. Scott and E. Jakobsson, *Biophys. J.*, 1995, **69**, 1230–1245.
54 W. F. van Gunsteren, *GROMOS. Groningen Molecular Simulation Program Package*, University of Groningen, Groningen, 1987.
55 W. L. Jorgensen and J. Tiradorives, *J. Am. Chem. Soc.*, 1988, **110**, 1657–1666.
56 J. Hermans, H. J. C. Berendsen, W. F. Vangunsteren and J. P. M. Postma, *Biopolymers*, 1984, **23**, 1513–1518.
57 B. Hess, H. Bekker, H. J. C. Berendsen and J. Fraaije, *J. Comput. Chem.*, 1997, **18**, 1463–1472.
58 S. Miyamoto and P. A. Kollman, *J. Comput. Chem.*, 1992, **13**, 952–962.
59 P. Schofield and J. R. Henderson, *Proc. R. Soc. London, Ser. A*, 1982, **379**, 231–246.
60 J. P. Ryckaert, G. Ciccotti and H. J. C. Berendsen, *J. Comput. Phys.*, 1977, **23**, 327–341.
61 K. A. Dill and P. J. Flory, *Proc. Natl. Acad. Sci. U. S. A.*, 1980, **77**, 3115–3119.
62 P. S. Niemela, S. Ollila, M. T. Hyvonen, M. Karttunen and I. Vattulainen, *PLoS Comput. Biol.*, 2007, **3**, e34.
63 H. J. Risselada and S. J. Marrink, *Phys. Chem. Chem. Phys.*, 2009, **11**, 2056–2067.
64 J. Sonne, F. Y. Hansen and G. H. Peters, *J. Chem. Phys.*, 2005, **122**.
65 S. Ollila, *Helsinki University of Technology*, 2006.